Digital signal processing for coherent multi-level modulation formats

(Invited Paper)

Xiang Zhou

AT&T Labs-Research, 200 Laurel Ave South, Middletown, NJ 07748, USA

E-mail: zhoux@research.att.com

Received May 26, 2010

This paper presents a review on the recent progress of digital signal processing (DSP) in the high-speed optical transmission system using single-carrier based multi-level modulation formats. The principle of several digital phase and polarization tracking algorithms recently proposed and demonstrated for future spectrally-efficient optical transmission system are discussed in detail. A novel DSP-based interference mitigation algorithm for the single-ended coherent receiver has been included. Recent technology advance on transmitter-side DSP such as digital pulse-shaping, pre-equalization and digital nonlinear compensation has also been discussed.

OCIS codes: 060.0060, 030.0030.

doi: 10.3788/COL20100809.0863.

1. Introduction

With the advancement of fast electrics, digital signal processing (DSP) has been playing an increasingly important role in the high-speed optical transmission system. The first generation of DSP introduced in the 10-Gb/s direct-detection system was mainly used for electrical chromatic dispersion (CD) compensation by employing either digital pre-distortion at the transmitter[1] or maximum likelihood sequence (MLSE) detection at the receiver[2]. With the recent development of advanced digital phase[3,4], and polarization tracking algorithms[5–7], the second generation of DSP has basically enabled the practical implementation of coherent detection. Such DSP-enabled coherent detection (i.e., digital coherent detection) not only allows electrical compensation or mitigation of several optical impairments such as CD, polarization mode dispersion (PMD), and narrow optical filtering effects, it also allows us to use a universal receiver front-end for the optimal reception of various multi-level modulation formats. The use of advanced multi-level modulation formats and digital coherent detection has resulted in significant improvement of spectral efficiency (SE) and the overall fiber capacity in the recent several years[8–13].

The concept of a typical digital coherent receiver is illustrated in Fig. 1. For such a receiver, the incoming optical field is coherently mixed with a local oscillator (LO) through a polarization- and phase-diverse 90° hybrid. This hybrid separates the in-phase and quadrature components of the received optical field in both the x and y polarizations, which can then be detected using either four balanced photodetectors or four single-ended photodetectors with a high LO-to-signal power ratio (LOSPR). The single-ended coherent receiver can achieve a similar sensitivity as the balanced receiver as long as the LOSPR is high enough[8]. The photo-detected analog electrical signals are digitized and then processed at the DSP unit, which is the heart of a digital coherent receiver. The DSP part typically consists of two "fixed" or slowly adaptable frequency-domain based digital equalizers for large amount of CD compensation (for the systems without using inline optical dispersion compensation), four butterfly-configured fast adaptive digital finite impulse response (FIR) filters for polarization tracking, and a carrier recovery unit for signal-LO frequency offset and carrier phase estimation. Recently it has been shown that optical front-end errors such as the interference caused by the direct detection of the signal components in the single-ended coherent receiver and quadrature imbalance can be effectively mitigated or corrected by using novel digital methods[8,14]. To increase the system tolerance toward amplified spontaneous emission (ASE) noise, soft-decision forward error correction (FEC) code is highly likely to be implemented in the 100 Gb/s and above optical transmission systems. Using DSP to compensate or mitigate fiber nonlinear effects is also a very active research topic[15–18].

In addition to the receiver-side DSP for the coherent detection and optical impairments compensation, advanced transmitter-side DSP such as digital pulse shaping and spectrum pre-emphasis has recently been demonstrated with high-order multi-level modulation formats[12,19]. It is shown that pre-equalization of deterministic (or slowly-varying) band-limiting effects at the transmitter is better than post-equalization at the receiver[12]. With DSP introduced at the transmitter, different modulation formats and therefore data rates can be generated simply by changing the software. Such software-reconfigurable capability can be very useful for the network with very diverse reaches and capacity demands.

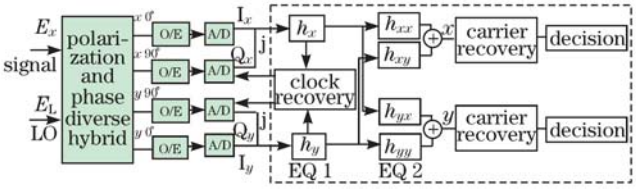

Fig. 1. Illustration of a typical digital coherent receiver.

1671-7694/2010/090863-08

This paper reviews the recent progress of DSP in the high-speed optical transmission system using single-carrier based multi-level modulation formats and intradyne detection. The principle of several phase and polarization tracking algorithms recently proposed and demonstrated for high-spectral-efficiency optical transmission is discussed. A novel DSP-based interference mitigation algorithm for the single-ended coherent receiver has been included. Recent progress on transmitter-side DSP such as digital pulse-shaping and pre-equalization and digital nonlinear compensation has been discussed.

The remainder of this paper is organized as follows. Section 2 is devoted to an interference mitigation algorithm for the single-ended coherent receiver. In Section 3 several polarization tracking algorithms recently demonstrated for high spectral efficiency optical transmission using multi-level modulation formats and intradyne detection are discussed. Digital carrier frequency and phase recovery algorithms are presented in Section 4. A brief discussion on transmitter-side DSP and digital nonlinear compensation is given in Section 5. Conclusion is presented in Section 6.

2. Receiver interfernce mitigation algorithm

A digital coherent receiver using single-ended photodetection may have a significant cost advantage over a coherent receiver using balanced detection. However, this cost advantage comes with a problem that the direct square-law detection of the modulated signal will interfere with the original signal, which may severely degrade the performance of DSP-based dispersion compensation, polarization recovery, and PMD compensation, especially for high-level modulated optical signals. Traditionally, this interference is mitigated by using a very large value of LOSPR[20]. Alternatively, a DSP-based method can be used to address this problem[8].

For a polarization- and phase-diverse coherent receiver using single-ended photodetection, the signal powers received by the photodetector (PD) in the in-phase (0°) and quadrature branches (90°) at one of the two polarizations can be given by

$$P_{\rm I}(t) = P_{\rm S}(t) + P_{\rm L}(t) + 2\sqrt{P_{\rm S}(t)P_{\rm L}(t)}\cos\left[\theta(t)\right], \quad (1)$$

$$P_{\rm Q}(t) = P_{\rm S}(t) + P_{\rm L}(t) + 2\sqrt{P_{\rm S}(t)P_{\rm L}(t)}\sin\left[\theta(t)\right], \quad (2)$$

where $P_{\rm S}(t)$ and $P_{\rm L}(t)$ denote the signal and LO power, respectively; $\theta(t)$ represents the relative phase between the received optical signal and the reference optical signal (i.e., the LO). After photodetection and analog-to-digital conversion, the digitized electrical signal with alternating current (AC) coupling can be approximated as

$$I_{\rm I}(n) \approx \tilde{I}_{\rm S}(n) + 2\sqrt{I_{\rm S}(n)I_{\rm L}(n)}\cos\left[\theta(t_{\rm n})\right], \quad (3)$$

$$I_{\rm Q}(n) \approx \tilde{I}_{\rm S}(n) + 2\sqrt{I_{\rm S}(n)I_{\rm L}(n)}\sin\left[\theta(t_{\rm n})\right], \quad (4)$$

where $I_{\rm S}(n)$ and $I_{\rm L}(n)$ denote the photodetected signal and LO at the nth sampling time, respectively; $\tilde{I}_{\rm S}(n)$ is the AC component of $I_{\rm S}(n)$. The basic idea of the proposed DSP algorithm is to find the approximate value of $\tilde{I}_{\rm S}(n)$ with the knowledge of $I_{\rm I}(n)$ and $I_{\rm Q}(n)$. Assuming that $I_{\rm L}(n) \gg I_{\rm S}(n)$, then to a first-order approximation we can have

$$I_{\rm I}(n) \approx 2\sqrt{I_{\rm S}(n)I_{\rm L}(n)}\cos\left[\theta(t_{\rm n})\right], \quad (5)$$

$$I_{\rm Q}(n) \approx 2\sqrt{I_{\rm S}(n)I_{\rm L}(n)}\sin\left[\theta(t_{\rm n})\right]. \quad (6)$$

Note that $I_{\rm S}(n)$ and $I_{\rm L}(n)$ in expressions (5) and (6) can be expressed as

$$I_{\rm S}(n) = \overline{I}_{\rm S}(n) + \tilde{I}_{\rm S}(n), \quad (7)$$

$$I_{\rm L} \approx \bar{I}_{\rm L}, \quad (8)$$

where the bar over the symbols denotes the direct current (DC) component (i.e., time-averaged portion). From expressions (5)−(8) it can be found that

$$I_{\rm I}^2(n) + I_{\rm Q}^2(n) \approx 4\tilde{I}_{\rm S}(n)\bar{I}_{\rm L}(n) + 4\bar{I}_{\rm S}\bar{I}_{\rm L}, \quad (9)$$

$$\overline{I_{\rm I}^2 + I_{\rm Q}^2} = 4\bar{I}_{\rm S}\bar{I}_{\rm L}. \quad (10)$$

Using expression (9) and Eq. (10), the first-order approximation for $\tilde{I}_{\rm S}(n)$ is given by

$$\tilde{I}_{\rm S}^{(1)}(n) = \frac{I_{\rm I}^2(n) + I_{\rm Q}^2(n) - \overline{I_{\rm I}^2 + I_{\rm Q}^2}}{4\bar{I}_{\rm L}}. \quad (11)$$

Note that $\bar{I}_{\rm L}$ is a constant that only depends on the LO power and the receiver configuration. Its value can be determined easily by doing an initial calibration. Thus the first-order approximation for $\tilde{I}_{\rm S}(n)$ can be estimated with the knowledge of the received in-phase and quadrature components, $I_{\rm I}(n)$ and $I_{\rm Q}(n)$. A more accurate second-order approximation for $\tilde{I}_{\rm S}(n)$ can be found by simply replacing $I_{\rm I}(n)$ and $I_{\rm Q}(n)$ in expressions (5) and (6) by $I_{\rm I}(n) - \tilde{I}_{\rm S}^{(1)}(n)$ and $I_{\rm Q}(n) - \tilde{I}_{\rm S}^{(1)}(n)$.

The algorithm described above has been verified by both experiment and simulation. The experimental verification is based on an 8 ×114 Gb/s, 25 GHz-spaced dense wavelength division multiplexing (DWDM) system using return-to-zero (RZ) pulse-shaped polarization division multiplexing 8-phase shift keying (PDM-8PSK) modulation (experimental setup is described in Ref. [8]). The launch power was chosen to be −2.5 dBm and the received optical signal-to-noise ratio (OSNR) of channel 4 after 640-km transmission was 25 dB (in 0.1-nm noise bandwidth). Figure 2 shows the measured bit error rate (BER) of channel 4 versus various values of LOSPR after 640-km of transmission with three different post-processing scenarios: 1) without using the proposed DSP algorithm, 2) using the proposed algorithm with a first-order approximation, and 3) using the proposed algorithm with an approximation up to the second order. It can be seen that the proposed algorithm can reduce the required LOSPR by more than 7 dB. The simulation results are shown in Fig. 3. This simulation is based on a single-channel 114-Gb/s PDM-8PSK system with 640-km transmission reach and 100-ps first-order PMD. The receiving OSNR is assumed to be 18 dB. For comparison, the result with balanced detection is also shown in Fig. 3 as a reference. It can be seen that the simulated results reasonably agree with the experimental results

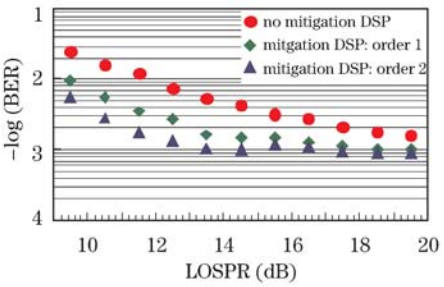

Fig. 2. Measured BER versus LOSPR with different processing scenarios.

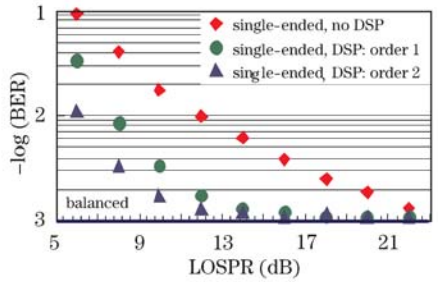

Fig. 3. Simulated results with 114-Gb/s PDM-8PSK using different detection and processing scenarios.

shown in Fig. 2. We can also see that, with the proposed algorithm, the single-ended coherent receiver can achieve a similar performance as the balanced receiver without using a very high LO power.

Finally we should mention that, unlike balanced detection that rejects both the in-band and out-of-band interference caused by the direct power-law detection of the signal components, the algorithm described above is only effective for in-band interference mitigation. For the reception of wavelength division multiplexing (WDM) signals, this implies that balanced detection may not need optical filter before the receiver but optical filter is usually necessary for the single-ended detection.

3. Polarization tracking algorithms

The four butterfly-configured adaptive digital equalizers shown in Fig. 1 are used for polarization recovery and de-multiplexing, PMD compensation, as well as residual CD compensation. Other linear distortions such as optical filtering effects can also be compensated or mitigated by this adaptive equalization. $T/2$–spaced time-domain or frequency-domain FIR filters are commonly used as the equalizers to achieve the best performance. But a $(2/3)T$-spaced FIR filter may also be used to reduce the receiver complexity. For this fast adaptive equalization, the classic stochastic gradient algorithm (see Fig. 4) is commonly used for filter coefficients updating. In order to apply the stochastic gradient algorithm, however, we need to first decide how to calculate the feedback error signal (denoted as ε_x and ε_y in Fig. 4), which is the key problem for any feedback-based equalizer, because in essence the stochastic gradient algorithm minimizes the time averaged feedback error.

The feedback error signal can be easily calculated if the system sends the training sequence periodically. This training based method has the advantage of fast

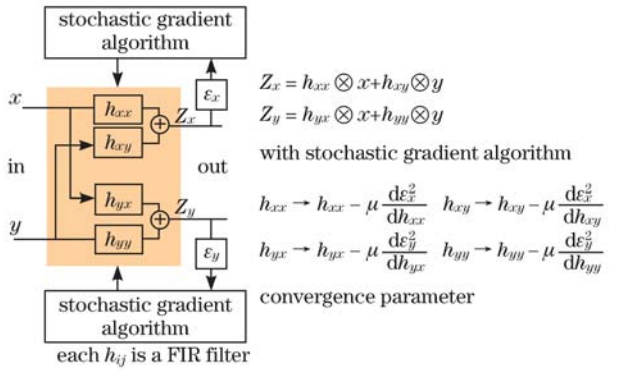

Fig. 4. Illustration of stochastic gradient algorithm, where x, y denote the two orthogonal polarizations and $\varepsilon_{x,y}$ denotes the feedback error signals.

convergence and optimal signal-to-noise ratio (SNR) performance[21], but how to achieve the initial time synchronization of the training sequence is a potential problem. In addition, the overhead required by the training based solution will consume bandwidth and therefore decrease the achievable spectral efficiency. For the case that there is no training sequence, blind equalization can be realized by looking for either the modulation properties or the statistical properties of the received signal. Because blind equalization does not consume extra bandwidth, higher spectral efficiency can be achieved by using blind equalization. This may be a significant advantage for future bandwidth-constrained high-speed optical communication systems.

First let us look at the blind equalization algorithms based on the special modulation properties. The most famous one of this type is the constant modulus algorithm (CMA)[22]. If we use $Z_{x,y}(i)$ to denote the equalized received symbols (i is the symbol time index, and x and y denote the two orthogonal polarizations, respectively), the CMA calculates the feedback error signal based on a single reference circle of radius R in the complex plane (constant modulus) as

$$\varepsilon_{x,y}(i) = |Z_{x,y}(i)|^p - R^p, \tag{12}$$

where p is the order number and typically is chosen to be 2 to balance the convergence speed and stable-state SNR performance. The constant modulus R is given by $E|Z|^2 \big/ E|Z|$, where E denotes the statistical expectation. Using the stochastic gradient algorithm illustrated in Fig. 4, we can find the filter coefficients adaptation equation for each of the four FIR filters, as shown in Fig. 5. Note that $\hat{x}$ and $\hat{y}$ denote the complex conjugates of x and y, respectively. CMA works particularly well for modulation formats presenting constant amplitude such as M-ary phase shift keying (PSK), where it is often the only equalization algorithm. For modulation formats that do not present constant amplitude such as quadrature amplitude modulation (QAM), which are generally composed of multiple rings/modulus, however, the time-averaged error of CMA will not be reduced to zero, therefore extra noise will be introduced after equalization.

To improve the SNR performance for modulation formats that do not present constant amplitude, several

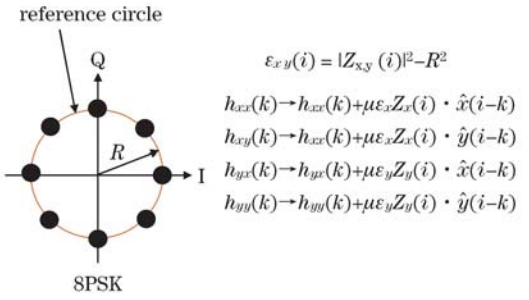

Fig. 5. Error signal and filter tap coefficients updating equations based on the classic second-order CMA.

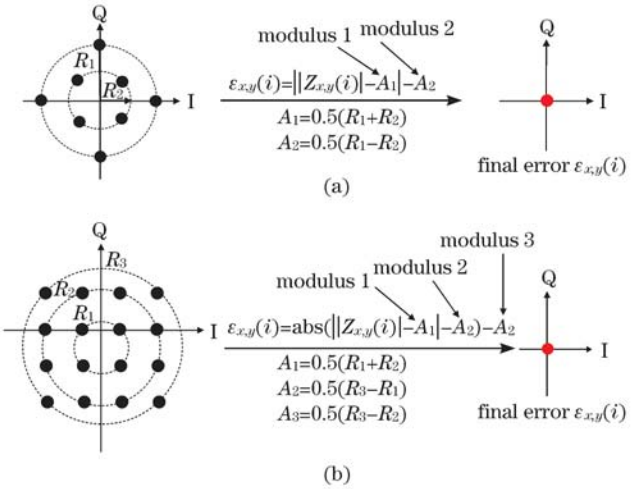

Fig. 6. Illustration of CMMA for (a) 8QAM and (b) 16QAM.

multi-modulus algorithms (MMAs) have recently been proposed[23−26], including the radius-directed algorithm (RDA)[25] and the cascaded multi-modulus algorithm (CMMA)[23]. RDA has been investigated before in the radio-frequency (RF) communication system[24] where one first makes decision on the ring that a received symbol most likely belongs to and then calculates the error signal using a CMA based on the knowledge of the correct ring radius

$$r_i, \text{i.e.}, \varepsilon_{x,y}(i) = |Z_{x,y}(i)|^p - r_i^p.$$

CMMA was proposed in a recent optical transmission experiment using polarization-multiplexed (PM) 8QAM modulation format. Experimental demonstration of this algorithm with square 16QAM has also been reported[23]. For this algorithm, multiple reference circles are introduced in a cascaded way such that the final error approaches zero for an ideal signal. By using 8QAM and 16QAM as two examples, Fig. 6 illustrates how to calculate the error signal using the proposed CMMA. The corresponding filter tap weight updating equations resulting from the stochastic gradient algorithm are given as follows:

$$h_{\mathrm{xx}}(k) \rightarrow h_{xx}(k) + \mu\varepsilon_x(i)e_x(i)\hat{x}(i-k), \quad (13)$$
$$h_{\mathrm{xy}}(k) \rightarrow h_{yx}(k) + \mu\varepsilon_x(i)e_x(i)\hat{y}(i-k), \quad (14)$$
$$h_{\mathrm{yx}}(k) \rightarrow h_{yx}(k) + \mu\varepsilon_y(i)e_y(i)\hat{x}(i-k), \quad (15)$$
$$h_{\mathrm{yy}}(k) \rightarrow h_{yy}(k) + \mu\varepsilon_y(i)e_y(i)\hat{y}(i-k). \quad (16)$$

For 8QAM, $e_{x,y}(i)$ is given by

$$e_{x,y}(i) = \mathrm{sign}(|Z_{x,y}(i)| - A_1) \cdot \mathrm{sign}(Z_{x,y}(i)). \quad (17)$$

For 16QAM, $e_{x,y}(i)$ is given by

$$e_{x,y}(i) = \mathrm{sign}\left(C_{x,y}(i)\right) \cdot \mathrm{sign}\left(B_{x,y}(i)\right) \cdot \mathrm{sign}\left(Z_{x,y}(i)\right), \quad (18)$$
$$B_{x,y}(i) = |Z_{x,y}(i)| - A_1, \quad (19)$$
$$C_{x,y}(i) = |B_{x,y}(i)| - A_2. \quad (20)$$

In the above equations, sign (x) is a sign function given by $x/|x|$, μ is a convergence parameter.

It has been shown that the above described MMAs can achieve significantly better SNR performance than CMA for both 8QAM[8,23] and 16QAM[26], but reduced robustness in filter convergence has also been observed[11]. This is due to the fact that the MMAs directly (RDA) or indirectly (CMMA) rely on the correct decisions regarding the transmitted ring radii; since the ring spacing in QAM is generally smaller than the minimum symbol spacing (see Fig. 6), these decisions show a significant number of errors for heavy noise loading and/or for severe signal distortions. One solution to this problem is to use the classic single-ring CMA at the starting stage for pre-convergence; once pre-convergence is achieved, the system is then switched to a MMA for stable-state operation. Because MMAs are backward-compatible to the single-ring CMA, adding a CMA at the starting stage does not add into any implementation complexity as compared to the case that uses a standalone MMA. For high-order QAM such as 32QAM or 64QAM, the implementation complexity of a MMA can be reduced by only selecting the inner two or three rings for the error signal calculation[12]. Because the ring spacing between the inner two or three rings is generally greater than the other rings with greater radii, this scenario can also improve the convergence robustness.

Another way to improve the equalizer SNR performance is to use the CMA at the starting stage for pre-convergence and the decision-directed least mean square (DD-LMS) for the stable-state operation. The standard DD-LMS calculates the error signal by

$$\varepsilon_{x,y}(i) = Z_{x,y}(i) - d_{x,y}(i), \quad (21)$$

where $d_{x,y}(i)$ is the finally decided signal after carrier frequency and phase recovery based on the optimal QAM decision boundary. The filter tap coefficients are updated based on the following equations:

$$h_{xx}(k) \rightarrow h_{xx}(k) - \mu\varepsilon_x(i)\hat{x}(i-k), \quad (22)$$
$$h_{xy}(k) \rightarrow h_{yx}(k) + \mu\varepsilon_x(i)\hat{y}(i-k), \quad (23)$$
$$h_{yx}(k) \rightarrow h_{yx}(k) + \mu\varepsilon_y(i)\hat{x}(i-k), \quad (24)$$
$$h_{yy}(k) \rightarrow h_{yy}(k) + \mu\varepsilon_y(i)\hat{y}(i-k). \quad (25)$$

Unlike the CMA/MMA where the equalization and the carrier recovery can be implemented independently within different functional blocks, the CMA/DD-LMS needs to implement the equalization and the carrier recovery and decision into a single functional block/loop. Because an estimation of initial carrier frequency offset and symbol phase is required before the start of filter

adaptation, the standard DD-LMS may fail if the residual phase error is too large due to a poor CMA pre-equalization. To overcome this problem, a modified DD-LMS algorithm has been proposed[11,27]. This modified DD-LMS uses a phase-independent error signal as

$$\varepsilon_{x,y}(i) = |Z_{x,y}(i)|^2 - |d_{x,y}(i)|^2 . \quad (26)$$

From Eq. (26) one can see the error signal is calculated based only on the radial information which is similar to RDA. But unlike RDA where the radius decision is made based on the ring boundary, the modified DD-LMS makes this decision based on the optimal QAM decision boundary after carrier frequency and phase recovery. Since the ring spacing in QAM is generally smaller than the minimum symbol spacing, DD-LMS can achieve better SNR performance than MMAs. It is found that the performance difference is relatively small for 8QAM[10] and 16QAM[26], but it increases as the modulation level increases[12].

All the equalization algorithms discussed above require the detailed knowledge of the used modulation formats. These algorithms allow us to decouple communication intermixed signals without the knowledge of the decomposition matrix of the transmission channels. Alternatively, if one can predefine the decomposition matrix with a reduced set of parameters, communication intermixed signals in principle can be separated by looking for the statistical properties of the received signal without knowing the exact nature of the received signal such as the used modulation formats. If the original signals before mixing/transmission are statistically independent, which is usually the case for the practical system, independent component analysis (ICA)[28−30] can be used to separate the mixed signal. ICA relies on the assumption of statistical independence of the input signals to evaluate the transformation matrix only from the output signals. In the case of polarization demultiplexing, there are two inputs and two outputs. The ICA criterion can be expressed as

$$p_{xy}(E_x, E_y) = p_x(E_x)p_y(E_y), \quad (27)$$

where p_{xy} is the joint probability density function (PDF) of two orthogonal polarizations while p_x and p_y are marginal PDFs of x and y polarizations, respectively. In practice, instead of PDFs, high order cumulants are used to determine statistical independence. According to the central limit theorem, the statistics of a mixed signal tend towards Gaussian distribution. In other words, independent signals are less Gaussian compared with their mixtures. Since high order cumulants of Gaussian signals are all zero, they can be used in ICA to determine the Gaussianity of a signal.

The use of ICA for blind polarization de-multiplexing has recently been reported for both QPSK and 16QAM[30] by assuming negligible PMD and polarization dependent loss (PDL). Figure 7 shows the experimental results with 16QAM. For this work, the fourth order marginal cumulant is used as the indicator to find independent components and the transmission decouple matrix is assumed to be a unitary matrix as

$$\mathbf{U} = \begin{pmatrix} \cos\alpha & \sin\alpha \mathrm{e}^{\mathrm{j}\theta} \\ -\sin\alpha \mathrm{e}^{-\mathrm{j}\theta} & \cos\alpha \end{pmatrix}. \quad (28)$$

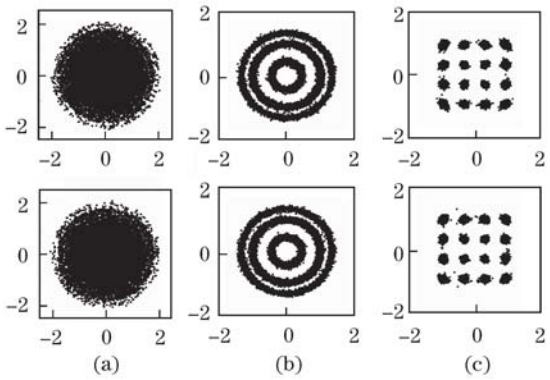

Fig. 7. Signal constellation plots of x (upper) and y (bottom) polarizations for 16-QAM data (a) before polarization demultiplexing, (b) after polarization demultiplexing, and (c) after phase estimation.

But for a real fiber transmission system having significant PMD and PDL, how to apply ICA without using the knowledge of the used modulation formats is still facing significant challenges.

4. Phase tracking algorithms

Decision-directed or decision feedback based digital phase-locking loop (PLL) is widely used for carrier phase recovery in the RF communication systems because a RF carrier phase typically varies very slowly. In the high-speed optical communication system, however, the phase of the optical carrier changes much faster than its RF counterpart, therefore feed-forward based phase recovery is necessary for the practical implementation that uses parallel and pipeline architecture. Because the frequency drift is much slower than the phase change, digital PLL can still be used in the high-speed optical communication system for signal-LO frequency offset estimation.

For M-PSK modulation formats, the most widely used feed-forward carrier recovery algorithm is based on the classic Viterbi-Viterbi algorithm[31], i.e., the Mth power algorithm. For this algorithm, the signal is first raised to the Mth-power to remove the data modulation (M=4 for QPSK, M=8 for 8PSK) and then the frequency offset between the transmitted signal and the LO is decided from the speed of the phase rotation of the resulting signal. After the frequency offset is removed, the frequency-recovered signal is raised to Mth-power again to remove the data modulation. Because the laser phase noise changes more slowly than the other additive noise contributions such as ASE noise, the phase noise can be estimated by averaging over multiple adjacent symbols.

The classic Mth-power algorithm requires a Mth-power operation to remove the data modulation for the phase estimation. It is recently found that there exists a simpler angle-based method for M-PSK modulation[32]. With $Z(i)$ denoting the received M-PSK symbol, the angle-based method estimates the carrier phase by using two cascaded modulo operation given by

$$\theta_i = (\arg(Z(i)) \bmod 2\pi) \bmod \pi/M. \quad (29)$$

It can be seen that the positive angle θ_i is independent of the M-PSK modulation, a property that it shares with

$(Z(i))^M$ and to which it is related as follows:

$$\theta_i = \frac{1}{M}\left(\arg\left(Z^M(i)\right) \mod 2\pi\right). \tag{30}$$

Because the angle-based phase estimation removes the multiplier operation, it is more efficient than the Mth-power algorithm in terms of hardware implementation.

The above described Mth-power algorithm as well as the angle-based algorithm in principle can be used for the phase estimation of M-QAM modulation formats by employing dedicated symbols that have equal phase spacing[33]. Because only a small portion of the current symbols is used for the phase estimation for high-order M-QAM, this method is inherently poor in terms of laser linewidth tolerance. To improve the tolerance toward the laser phase noise for high-order M-QAM, a blind phase search (BPS) algorithm[34] has been proposed. This method not only employs a feed-forward configuration but also involves all the current symbols for the phase estimation, and therefore can achieve better phase noise tolerance than the Viterbi-Viterbi algorithm. But the problem associated with this method is its complexity; the required number of test phase angles increases with the modulation level and can be significant for high-order M-QAM (for example, >32 is required for square 64QAM[34]).

To reduce the implementation complexity of the BPS algorithm, an improved multi-stage hybrid BPS/ML (maximum likelihood) algorithm has recently been proposed[35]. The proposed method introduces multiple cascaded phase recovery stages by employing a coarse BPS in the first stage and a constellation-assisted ML carrier phase estimate in the following stages. As compared to the single-stage BPS method, it is shown that the improved algorithm can reduce the required computaion power by more than a factor of 3 for square 64QAM.

The block diagram for the proposed multi-stage feed-forward carrier recovery method is shown in Fig. 8, where a two-stage configuration is shown as an example. In the first stage, a coarse BPS method is used to find the rough

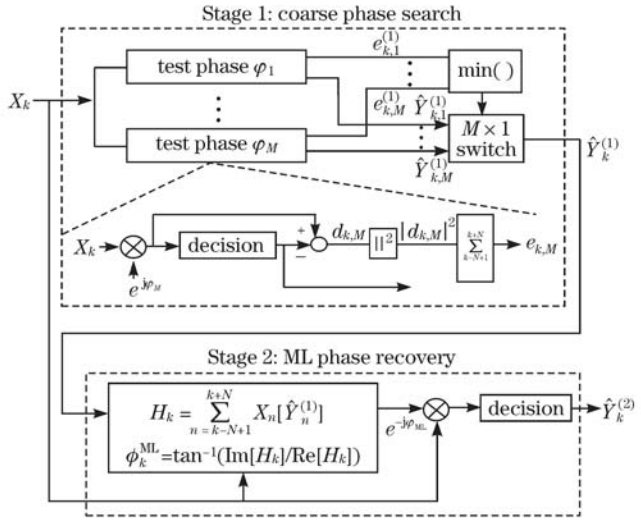

Fig. 8. Schematic illustration of the proposed multi-stage feed-forward carrier recovery algorithm.

location of the optimal phase angle. Decisions made following this rough phase estimation are then used for more accurate phase estimation through a ML phase estimate in the second stage.

First let us discuss the coarse BPS method. We denote the digitized signal (one sample per symbol) entering into the carrier phase recovery module as X_k. As described in Ref. [34], to recover the carrier phase in a pure feed-forward approach, BPS requires X_k to be rotated by multiple test carrier phase angles φ_m with

$$\varphi_m = \frac{m-1}{M}\cdot\frac{\pi}{2}, m \in \{1, 2, \cdots M\}. \tag{31}$$

Then all rotated symbols are fed into a decision circuit and the squared distance $|d_{k,m}|^2$ to the closest constellation point is calculated. In order to remove distortions from additive noise, the distances of $2N$ consecutive test symbols rotated by the same carrier phase angle φ_m are summed up:

$$e_{k,m} = \sum_{n=-N+1}^{N} |d_{k-n,m}|^2, \tag{32}$$

and the "optimum" phase angle is determined by searching for the minimum sum of the distance values. As the decoding has already been executed in Eq. (32), the decoded output symbol $\hat{Y}_k^{(1)}$ can be selected from the $\hat{Y}_{k,m}^{(1)}$ by a switch controlled by the index of the minimum distance sum.

The decoded/decided signal $\hat{Y}_k^{(1)}$ based on this rough phase estimation (along with the original signal X_k) is then fed into the second stage where a ML phase estimate is employed to find a more accurate phase estimate ϕ_k^{ML} by[36]

$$H_k = \sum_{n=k-N+1}^{k+N} X_n \left[\hat{Y}_n^{(1)}\right]^*,$$
$$\phi_k^{\mathrm{ML}} = \tan^{-1}\left(\mathrm{Im}\left[H_k\right]/\mathrm{Re}\left[H_k\right]\right). \tag{33}$$

The decoded signal $\hat{Y}_k^{(2)}$ based on this ML phase estimate along with the original signal X_k may be passed into another ML phase estimation stage to further refine the phase estimation. Because the reference signal used for the above ML phase estimation is extracted from the same block of data based on pure knowledge of the constellation diagram, we will refer to this technique as the "constellation-assisted ML phase estimate". The required processing for this ML phase estimate ($2N$ complex multipliers, 1 real multiplexer, $2N$ real adders, $2N$ decision blocks, 1 tangent and $2N$ phase rotation for $2N$ signals using simple block-by-block averaging method is equivalent to testing one phase angle using the BPS method (per test phase the BPS method requires $2N$ complex multipliers, $2N+1$ real adders, $2N$ decision blocks, 1 comparator, $2N$ selectors, and $2N$ phase rotation).

The effectiveness of the proposed method has been verified by numerical simulation using square 64QAM as an example. Figure 9 gives the simulated BER versus the equivalent number of test phase angles for three different

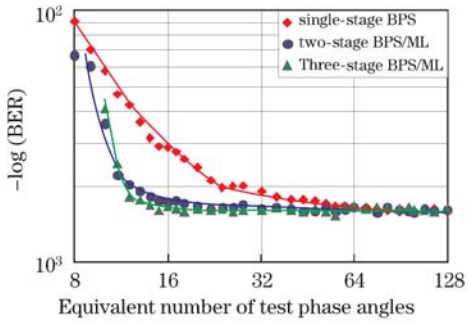

Fig. 9. Simulated results on the required equivalent number of test phase angles for square 64 QAM using three different feed-forward carrier phase recovery scenarios.

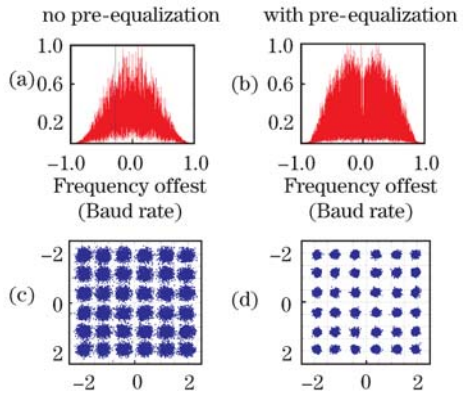

Fig. 10. Baseband 36QAM spectrum (a) without and (b) with pre-equalization received constellation diagrams (c) without and (d) with pre-equalization.

feed-forward phase recovery scenarios: the single-stage BPS method, the proposed two- and three-stage hybrid BPS/ML phase recovery schemes. For these investigations, the laser phase noise for both the signal source and the LO is assumed to be 100 kHz. The received OSNR in 0.1-nm noise bandwidth is 28 dB. At such a laser linewidth and OSNR level, the optimal phase block/filter length for the BPS method and the proposed hybrid BPS/ML method are very close and are between 24 and 36. The results shown in Fig. 2 are based on a phase block length of 28 and the BER is estimated based on 4.8×10^5 bits of information. Note that differential encoding/decoding has been applied to solve the $\pi/2$ phase ambiguity problem. From Fig. 2 one can find that, to achieve a performance that is close to the optimum, the single-stage BPS method needs to test about 64 different phase angles, while the proposed three-stage hybrid BPS/ML algorithm only needs to equivalently test 18 different phase angles (14 test phase angles used in the first coarse BPS stage plus two cascaded ML phase estimation stages), resulting in a reduction of computational effort by more than a factor of 3.

5. Discussions

Although most of the recently reported high-speed coherent optical transmission experiments employed DSP only at the receiver side, it is expected that better performance can be achieved by employing DSP at both the transmitter and the receiver. As is demonstrated in the recent 64-Tb/s optical transmission experiment using PDM-36QAM modulation format[12], pre-equalization of deterministic transmitter-side side band-limiting effects is better than post-equalization because post-equalization will enhance the noise components and therefore degrades the SNR performance (see Fig. 10). Digital pre-equalization may also be very useful for the mitigation of optical impairments caused by cascaded narrow optical filtering effects as well as polarization-dependent loss along the optical link using multiple optical amplifiers and wavelength selective switches. In addition, digital transmitter gives us much more flexibility for pulse shaping[12,37]. For example, raised-cosine pulse shaping can be realized by using a digital transmitter to reduce WDM crosstalk and/or increase the tolerance toward narrow filtering effects[12]. With DSP introduced at the transmitter, different modulation formats and therefore data rates can be generated simply by changing the software. Such software-reconfigurable capability can be very useful for the network with very diverse reaches and capacity demands.

Using digital method to compensate or mitigate the fiber nonlinear effects is currently a very active research field. The proposed methods include digital pre-compensation[15], digital backward propagation[16,17] as well as a maximum *a posterior* (MAP) detection algorithm[18]. However, these methods generally work well only for single-channel transmission or a WDM system with negligible inter-channel fiber nonlinear effects[38]. For the realistic terrestrial WDM system with wavelength-routing capability and strong (or not small) inter-channel fiber nonlinear effects, how to significantly improve the fiber nonlinear tolerance using digital methods remains very challenging, if not impossible.

6. Conclusions

As the complementary metal-oxide semiconductor (CMOS) capability continues to improve, advanced DSP is becoming more and more important in the high-speed optical transmission systems. Advanced DSP algorithms in combination with intradyne detection has made it possible for cost-effective implementation of fast polarization and phase tracking. This in turn enables us to use advanced multi-level and multi-dimensional modulation formats to increase the spectral efficiency for very-high-speed optical transmission.

For the blind polarization tracking algorithms, it is shown that CMA can be used as the standalone equalization algorithm for M-PSK. But two-stage CMA/MMA or CMA/DD-LMS has to be employed for the M-QAM modulation formats. For the carrier recovery, carrier-LO frequency offset can be estimated by using the traditional digital PLL but the carrier phase has to be estimated using feed-forward based methods. For M-PSK, linewidth-tolerant feed-forward carrier phase recovery can be realized by using either the Mth-power Viterbi-Viterbi algorithm or a more hardware-efficient angle-based algorithm. For M-QAM, linewidth-tolerant phase recovery can be achieved by using a single-stage BPS method or a multi-stage hybrid BPS/ML algorithm. It is shown that the multi-stage hybrid BPS/ML algorithm

is more computationally efficient than the single-stage BPS algorithm.

It is shown that pre-equalization of deterministic band-limiting effects is better than post-equalization. The use of digital transmitter gives us much more flexibility for pulse shaping. With DSP introduced at the transmitter, different modulation formats and therefore data rates can be generated simply by changing the software. Such software-reconfigurable capability can be very useful for the network with very diverse reaches and capacity demands.

We also show that some of the optical front errors can be effectively compensated by using novel digital methods.

References

1. M. Birk, X. Zhou, M. Boroditsky, S. H. Foo, D. Bownass, M. Moyer, and M. O'Sullivan, in *Proc. ECOC'06* Th2.5.6 (2006).
2. C. R. S. Fludger, J. E. A. Whiteaway, and P. J. Anslow, in *Proc. OFC'04* WM7 (2004).
3. M. G. Taylor, IEEE Photon. Technol. Lett. **16,** 674 (2004).
4. R. Noe, J. Lightwave Technol. **23,** 802 (2005).
5. Y. Han and G. Li, Opt. Express **13,** 7527 (2005).
6. R. Noe, IEEE Photon. Technol. Lett. **17,** 887 (2005).
7. S. J. Savory, Opt. Express **16,** 804 (2008).
8. X. Zhou, J. Yu, D. Qian, T. Wang, G. Zhang, and P. Magil, J. Lightwave Technol. **27,** 146 (2009).
9. X. Zhou and J. Yu, J. Lightwave Technol. **27,** 3641 (2009).
10. X. Zhou, J. Yu, M. Huang, Y. Shao, T. Wang, P. D. Magill, M. Cvijetic, L. Nelson, M. Birk, G. Zhang, S. Ten, H. B. Matthew, and S. K. Mishra, J. Lightwave Technol. **28,** 456 (2010).
11. P. J. Winzer, A. H. Gnauck, C. R. Doerr, M. Magarini, and L. L. Buhl, J. Lightwave Technol. **28,** 547 (2010).
12. X. Zhou, J. Yu, M. F. Huang, Y. Shao, T. Wang, L. Nelson, P. D. Magill, M. Birk, P. I. Borel, D. W. Peckham, and R. Lingle, in *Proc. OFC'10* PDPB9 (2010).
13. A. Sano, H. Masuda, T. Kobayashi, M. Fujiwara, K. Horikoshi, E. Yoshida, Y. Miyamoto, M. Matsui, M. Mizoguchi, H. Yamazaki, Y. Sakamaki, and H. Ishii, in *Proc. OFC 2010* PDPB7 (2010).
14. I. Fatadin, S. J. Savory, and D. Ives, IEEE Photon. Technol. Lett. **20,** 1733 (2008).
15. K. Roberts, C. Li, L. Strawczynski, M. O'Sullivan, and I. Hardcastle, IEEE Photon. Technol. Lett. **18,** 403 (2006).
16. X. Li, X. Chen, G. Goldfarb, E. F. Mateo, I. Kim, F. Yaman, and G. Li, Opt. Express **16,** 881 (2008).
17. E. Ip and J. M. Kahn, J. Lightwave Technol. **26,** 3416 (2008).
18. Y. Cai, D. G. Foursa, C. R. Davidson, J.-X. Cai, O. Sinkin, M. Nissov, and A. Pilipetskii, in *Proc. OFC 2010* OTuE1 (2010).
19. M. Yoshida, H. Goto, K. Kasai, and M. Nakazawa, Opt. Express **16,** 829 (2008).
20. C. R. S. Fludger, T. Duthel, D. Van Den Borne, C. Schulien, E.-D. Schmidt, T. Wuth, E. De Man, G. D. Khoe, and H. De Waardt, in *Proc. OFC 2007* PDP-22 (2007).
21. M. Kuschnerov, F. N. Hauske, K. Piyawanno, B. Spinnler, M. S. Alfiad, A. Napoli, and B. Lankl, J. Lightwave Technol. **27,** 3614 (2009).
22. D. N. Godard, IEEE Trans. Commun. **28,** 1867 (1980).
23. X. Zhou, J. Yu, and P. D. Magill, in *Proc. OFC 2009* OWG3 (2009).
24. M. J. Ready and R. P. Gooch, in *Proc. ICASSP'90* D11. 16 (1990).
25. H. Louchet, K. Kuzmin, and A. Richter, in *Proc. ECOC 2008* Tu.1.E.6 (2008).
26. I. Fatadin, D. Ives, and S. J. Savory, J. Lightwave Technol. **27,** 3042 (2009).
27. A. Spalvieri and R. Valtolina, "Data-aided and phase-independent adaptive equalization for data transmission systems" European Patent Application EP 1 089 457 A2 (2000).
28. P. Comon, Signal Processing **36,** 287 (1994).
29. A. Hyvärinen and E. Oja, Neural Networks **13,** 411 (2000).
30. X. B. Xie, F. Yaman, X. Zhou, and G. Li, IEEE Photon. Technol. Lett. **22,** 805 (2010).
31. A. J. Viterbi and A. M. Viterbi, IEEE Trans. Inf. Theory **29,** 543 (1983).
32. R. Peveling, T. Pfau, O. Aamczyk, R. Eickhoff, and R. Noé, IEEE Photon. Technol. Lett. **21,** 137 (2009).
33. M. Seimetz, in *Proc. OFC/NFOEC 2008* OTuM2 (2008).
34. T. Pfau, S. Hoffmann, and R. Noé, J. Lightwave Technol. **27,** 989 (2009).
35. X. Zhou, IEEE Photon. Technol. Lett. **22,** 1051 (2010).
36. J. G. Proakis, *Digital Communications* (4th edn.) (McGraw-Hill, New York, 2000) chap. 6, p. 348.
37. B. Châtelain, Y. Jiang, K. Roberts, X. Xu, J. C. Cartledge, and D. V. Plant, in *Proc. OFC 2010* OTuE6 (2010).
38. E. F. Mateo, X. Zhou, and G. Li, "Selective post-compensation of nonlinear impairments in polarization-division multiplexed WDM systems with different channel granularities" submitted to IEEE J. Sel. Top. Quantum Electron.